Revisiting the electrochemical formation, stability and structure of radical and biradical anionic structures in dinitrobenzenes

ARTICLE *in* ELECTROCHIMICA ACTA · NOVEMBER 2010

Impact Factor: 4.5 · DOI: 10.1016/j.electacta.2010.04.030

Electrochimica Acta 55 (2010) 8325–8335

Contents lists available at ScienceDirect

Electrochimica Acta

journal homepage: www.elsevier.com/locate/electacta

Revisiting the electrochemical formation, stability and structure of radical and biradical anionic structures in dinitrobenzenes

Lindsay S. Hernández-Muñoz[a], Felipe J. González[a], Ignacio González[b], Marilia O.F. Goulart[c], Fabiane Caxico de Abreu[c], Adriana Santos Ribeiro[c], Rogério Tavares Ribeiro[d], Ricardo L. Longo[d], Marcelo Navarro[d,*], Carlos Frontana[a,**]

[a] Departamento de Química, Centro de Investigación y Estudios Avanzados, Av. I.P.N. 2508. Col. San Pedro Zacatenco, 07360, D.F., Mexico
[b] Departamento de Química, Universidad Autónoma Metropolitana-Iztapalapa, Área de Electroquímica, Apartado Postal 55-534, 09340, D.F., Mexico
[c] Instituto de Química e Biotecnologia, Universidade Federal de Alagoas, Tabuleiro do Martins, Maceió, AL, 57072-970, Brazil
[d] Departamento de Química Fundamental, Universidade Federal de Pernambuco, Av. Prof. Luiz Freire, s/n, Cid. Universitária, Recife, PE, 50740-540, Brazil

ARTICLE INFO

Article history:
Received 30 October 2009
Received in revised form 5 April 2010
Accepted 6 April 2010
Available online 14 April 2010

Keywords:
Dinitrobenzenes
Dianion biradical
Inductive effect
Carbonyl reduction
Electron and spin densities
ESR-spectroelectrochemistry

ABSTRACT

The effects of the position of a second nitroaromatic group (*ortho vs. para vs. meta*) during reduction of nitrobenzenes were analysed. Cyclic voltammetric experiments in acetonitrile solution revealed that *ortho*-, *meta*- and *para*-dinitrobenzenes show two reversible reduction processes. An Electrochemical-Electron Spin Resonance (E-ESR) study showed that the corresponding radical anions of the *ortho* and *para* derivatives, electrogenerated during the first electron transfer uptake, remain the same even after the second monoelectronic process, increasing their intensity due to the presence of a comproportionation process ($A^{2-} + A \rightarrow 2A^{\bullet -}$). For the case of the *meta* derivative, the electrogenerated radical anion at the first reduction peak is consumed at the second reduction step, forming a secondary radical species. During the electrochemical study of methyl 3,5-dinitrobenzoate, two successive and reversible electron processes were also observed; however, in this case, a very rare biradical dianion structure was found. The use of ESR-spectroelectrochemistry shed some light on controversial aspects of nitroaromatic reduction, especially concerning the second and further waves. These results were corroborated and interpreted with quantum chemical calculations of the molecular and electronic structures, electron affinities and spin densities. As a result, electrochemical mechanisms are presented and discussed.

1. Introduction

Reduction of nitro compounds is an issue of high interest and has been subject of many electrochemical studies [1–4]. For instance, the reduction of molecules bearing two nitro groups has gained attention in recent years [5–8] mainly due to the effects occurring in the stabilization of the corresponding electrogenerated radical anions by interacting groups present in the structure, since this phenomenon is known to be dependent on the environment surrounding the radical anion and on the method employed for its formation [6–9]. This issue is relevant, in biological and pharmacological terms, once the stability of the electrogenerated radical species is related to the capacity of these species to induce the formation of reactive oxygen species, in the presence of oxygen and after reduction [2–4,10–12] that *in vivo* or *in cell* occurs via the action of nitroreductases [2,11,12].

Electron spin resonance (ESR) is one of the most important tools for analyzing the molecular and electronic structures of radical containing species [13–15]. These studies have a direct relationship with electrochemical data as such radicals (generally radical anions) are generated during many electrochemical processes. Particularly, polarography and electrolysis have been widely used to generate anion radical species, allowing the determination of the reduction potential at a specifically active electrochemical moiety, as well as furnishing thermodynamic parameters [13–15]. As a result, correlation between electrochemical and ESR data can lead to relevant information on the electronic structure of radical anions and their structural relaxation upon reduction processes [13,15]. For instance, electrochemical reduction of *meta*-, *para*- and *ortho*-dinitrobenzenes, using polarography, shows two reversible systems associated with two consecutive monoelectronic transfers, giving rise to the respective anion radical and dianion [13–15]. However, the ESR spectra present signals related, only, to the first reversible wave, indicating that after the second electron uptake, a

* Corresponding author.
** Corresponding author. Current address: Centro de Investigación y Desarrollo Tecnológico en Electroquímica, Parque Industrial Querétaro Sanfandila, Querétaro, C.P. 76703, Mexico. Tel.: +52 442 2116000x7849; fax: +52 442 2116001.
E-mail addresses: navarro@ufpe.br (M. Navarro), ultrabuho@yahoo.com.mx (C. Frontana).

0013-4686/$ – see front matter © 2010 Elsevier Ltd. All rights reserved.
doi:10.1016/j.electacta.2010.04.030

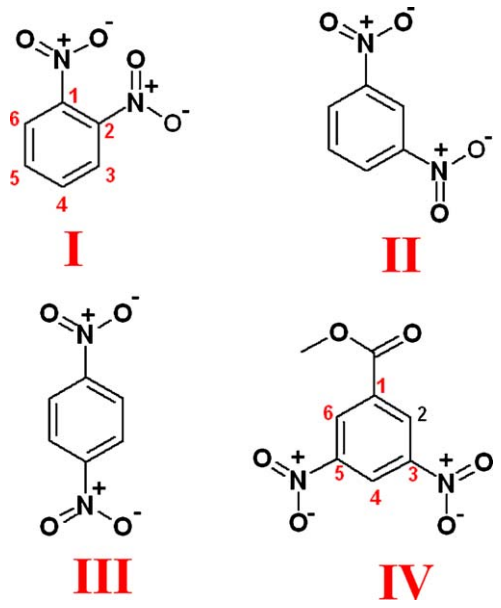

Fig. 1. Structures of the studied dinitrobenzenes: **I**: 1,2-dinitrobenzene; **II**: 1,3-dinitrobenzene; **III**: 1,4-dinitrobenzene; **IV**: methyl 3,5-dinitrobenzoate.

closed-shell system is formed. The same results were observed for the reduction of 4-amino-nitrobenzene; however, it was possible to detect the ESR signals of the protons at the amino group, which indicate a delocalization of the unpaired electron over the entire system [14].

Nitroaromatic compounds reduction give more stable radical anions or dianions than nitroaliphatic ones, due to charge delocalization by resonance effects, where in some cases, like *para*-dinitrobenzene, it is observed a large contribution of a quinonoidic type structure, which must have the major contribution to the true structure [8]. This stabilization may promote bond break at substituent-aromatic ring positions, such as bromine and iodine [16,17], or simple proton dissociation of phenol or carboxylic acid derivatives [18]. Reduction of dinitroaromatic compounds, similarly to the mononitroaromatic ones, are usually also followed by chemical reaction steps [19,20]. Despite of nitrobenzoyl being used as protecting group in reactions involving cathodic cleavage of C–O bond in benzoates [21], these compounds are far less studied than nitroaromatic compounds and usually the literature only reports data for the first reduction step.

In terms of electrochemical behavior, the reduction of molecules bearing two reducible nitro groups in aprotic media [1,5] (A), is represented in the next set of chemical equations:

$$A + e^- \rightleftharpoons A^{\bullet -} \quad E_1^0 \tag{1}$$

$$A^{\bullet -} + e^- \rightleftharpoons A^{2-} \quad E_2^0 \tag{2}$$

It is known that the potentials for these reactions are strongly dependent on the structural separation of both nitro groups [22] and also on the structural changes occurring during the electron transfer processes [23,24]. During studies concerning the electrochemical reduction of dinitroaryls, such as 1,2-dinitrobenzene (**I**), 1,3-dinitrobenzene (**II**) and 1,4-dinitrobenzene (**III**) (Fig. 1), evidence was found of complete delocalization of the spin of the radical anion $A^{\bullet -}$ (Eq. (1)) on both nitro groups through the aromatic ring [8,9]. Also, a second electron transfer yields a dianion species which, having no unpaired electrons, did not give an ESR signal. Thus, electron delocalization in radical anions is an important issue to consider and it is expected that such delocalization would be affected by the presence of substituents in the structure [25]. Indeed, an interesting compound to study is methyl 3,5-dinitrobenzoate (**IV**, Fig. 1), since the presence of the electron-withdrawing carbonyl group at *meta* position, should modify the reduction behavior of the nitro groups, albeit being also a reducible functionality in the molecule. Therefore, in this work, an electrochemical and ESR study of electrogenerated radical anions from a series of dinitrobenzenes was performed in order to evaluate how this delocalization determines the stability and the fate of radical anions. Also, a detailed analysis, using quantum chemical methods, of the molecular and electronic structure of the electrogenerated species is presented in order to corroborate and rationalize the behavior observed experimentally.

2. Experimental

2.1. Techniques and apparatus

Cyclic voltammetry experiments were performed using a PGSTAT 100 AUTOLAB Electrochemical Analyzer interfaced with a personal computer. Cyclic voltammetry experiments at several scan rates within the interval $0.1 \leq \nu \leq 100\,V\,s^{-1}$, were performed, applying IR drop compensation with R_u values determined from positive feedback measurements [26,27]. A glassy carbon disk electrode ($0.07\,cm^2$) was used as a working electrode, polished with 0.05 μm alumina powder (Buehler), and rinsed with acetone before each voltammetric run. A platinum wire and a commercial Saturated Calomel Electrode (SCE), the latter being separated from the medium with a salt bridge filled with the supporting electrolyte solution, were used as the auxiliary and reference electrodes, respectively. The potential values obtained are referred to the ferrocenium/ferrocene (Fc^+/Fc) couple, as recommended by IUPAC [28]. The potential for this redox couple, determined from voltammetric studies, was 0.41 V *vs.* SCE. The studies were carried out in an inert atmosphere by saturation with high purity argon gas (Praxair grade 5.0) at room temperature (~22 °C).

2.2. Reagents

1,2-Dinitrobenzene (**I**, >99%), 1,3-dinitrobenzene (**II**, 97%), 1,4-dinitrobenzene (**III**, 98%) and methyl 3,5-dinitrobenzoate (**IV**, 99%) Aldrich® (Fig. 1), were used as received, without further purification. Acetonitrile (CH_3CN) Merck® Spectroscopic grade, distilled from P_2O_5 and kept over molecular sieves (3 Å, Merck®) was used as solvent. Tetrabutylammonium hexafluorophosphate (n-Bu_4NPF_6, Aldrich®), recrystallized from ethanol, or tetraethylammonium tetrafluoroborate (Et_4NBF_4) were used as supporting electrolytes. All the solutions were purged with high purity argon (Praxair, Grade 5.0) for 25 min before each series of experiments.

2.3. Spectroelectrochemical-ESR measurements

ESR spectra were recorded in the X band (9.85 GHz), using a Brucker EMX Plus instrument with a rectangular TE_{102} cavity. A commercially available spectroelectrochemical cell (Wilmad) was used. A platinum mesh ($0.7\,cm^2$) was introduced in the flat path of the cell and used as a working electrode. Another platinum wire was used as a counter electrode. $Ag/AgNO_3$ $0.01\,mol\,L^{-1} + 0.1\,mol\,L^{-1}$ NBu_4PF_6 in acetonitrile was employed as the reference electrode. Potential control was performed with an AUTOLAB PGSTAT 100 potentiostat. The employed solutions were prepared in the same way as the ones used in the electrochemical studies.

2.4. ESR simulations

PEST WinSim free software Version 0.96 (National Institute of Environmental Health Sciences) was used to perform ESR spectra simulation, from the measured Hyperfine Coupling Constant values

(HFCC, a), and compared with the experimental ones. This program was also used to yield a-values, in the case when a direct measurement would be difficult under the spectra acquisition conditions.

2.5. Theoretical methods and computational procedure

All molecular structures were obtained with the B3LYP/6-311++G(d,p) method [29,30] implemented in the program Gaussian 03, Revision B.04 [31], using its default criteria for convergences without any symmetry constraints. These structures were characterized by their Hessian matrices calculated at the same level. For the non-planar conformations the dihedral angles defining the perpendicular conformations of the substituents were kept frozen during the geometry optimizations. For all open-shell systems the spin-unrestricted formalism (UB3LYP) was employed. The calculations of the hyperfine coupling constants (a-tensor) were performed with the UB3LYP/EPR-III method [32] as single point calculations at the UB3LYP/6-311++G(d,p) calculated structures, that is, UB3LYP/EPR-III//UB3LYP/6-311++G(d,p) level. The solvent effects (acetonitrile, $\varepsilon = 36.64$) were taken into account as single point calculations with dielectric continuum models PCM [33] and C-PCM [34] with the same program, using atomic radii generated by the united atom topological model [35] optimized at the PBE0/6-31G(d) level. The calculations of the g-tensors [36] were performed with the BLYP/TZ2P [37] method implemented in the ADF2009.1 program [38] using its default criteria for convergence and accuracy. The UB3LYP/6-311++G(d,p) calculated structures were employed. The spin-unrestricted (spin polarization) approach with the two-component zeroth-order regular approximation (ZORA) scalar relativistic correction [39] and spin–orbit (SO) correction within the collinear approximation [40] was used. The solvent effects were included via COSMO dielectric continuum model using the parameters for acetonitrile and Pauling atomic radii for building the solute cavity.

3. Results and discussion

3.1. Electrochemistry and ESR-spectroelectrochemistry dinitrobenzenes

Cyclic voltammograms of 1×10^{-3} mol L^{-1} solutions of **I**, **II** and **III** were obtained in the potential region between the open circuit potential (−0.26 V) and −2.7 V *vs.* Fc$^+$/Fc (Fig. 2).

The obtained voltammograms showed that the behavior of the studied compounds is characterized by the presence of two reduction processes – peaks Ic and IIc, Fig. 2 – associated with oxidation peaks Ia and IIa, respectively (peak potential values are presented in Table 1). From the anodic to cathodic peak potential separations, it was concluded that the first and second electron transfer processes in all compounds are a quasi-reversible uptakes **I**: $E_{pIa} - E_{pIc} = 65$ mV, $E_{pIIa} - E_{pIIc} = 122$ mV; **II**: $E_{pIa} - E_{pIc} = 71$ mV, $E_{pIIa} - E_{pIIc} = 94$ mV; **III**: $E_{pIa} - E_{pIc} = 74$ mV, $E_{pIIa} - E_{pIIc} = 88$ mV. Also, for compounds **I** and **II**, an additional oxidation signal (Peak IIa′), appears upon inverting the potential at values more negative than the corresponding peak IIc. The behavior described here is consistent with the reported two successive one-electron transfer processes occurring in dinitrobenzenes [5,22,41] (Eqs. (1) and (2)). In order to evaluate the capacity that these molecules have to generate stable radical anions, *in situ* spectroelectrochemical-ESR experiments were performed.

Upon applying a potential value intermediate between the potentials of peaks Ic and IIc, stable radical anion species were detected for the studied dinitrobenzenes **I**–**III** (Fig. 3). In general, it was observed for the electrogenerated radical anions that the corresponding hyperfine coupling patterns assigned to the H-nuclei

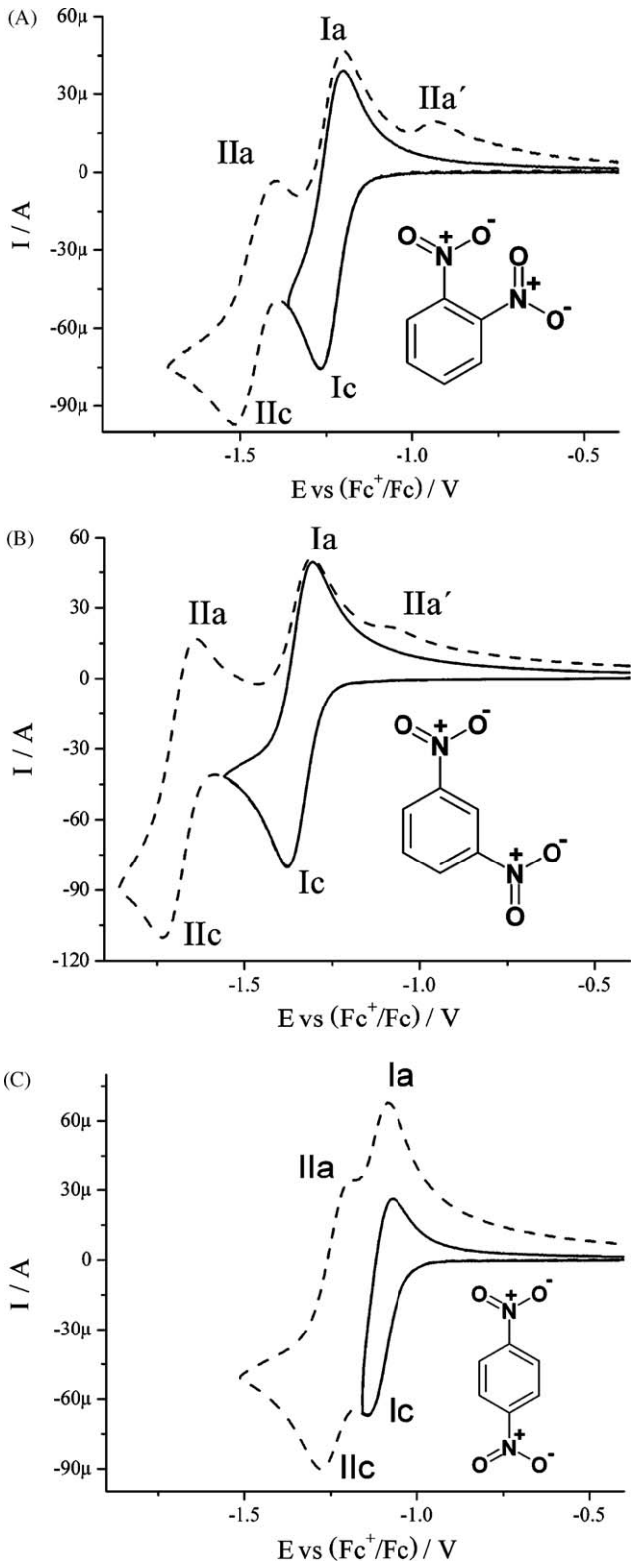

Fig. 2. Cyclic voltammograms of 1×10^{-3} mol L^{-1} of (A) **I**; (B) **II** and (C) **III** in 0.1 mol L^{-1} n-Bu_4NPF_6/CH_3CN. Voltammograms at different inversion potential conditions are shown. v: 100 mV s^{-1}. WE: glassy carbon (0.07 cm^2).

Table 1
Peak potential values, at 0.1 Vs^{-1}, of the dinitrobenzene derivatives **I–IV**.

Compound	E_p *vs.* (Fc^+/Fc)/V reduction signals	E_p *vs.* (Fc^+/Fc)/V oxidation signals
1,2-Dinitrobenzene (**I**)	$E_{pIc} = -1.269$ $E_{pIIc} = -1.519$	$E_{pIa} = -1.204$ $E_{pIIa} = -1.497$ $E_{pIIa'} = -0.932$
1,3-Dinitrobenzene (**II**)	$E_{pIc} = -1.377$ $E_{pIIc} = -1.735$	$E_{pIa} = -1.306$ $E_{pIIa} = -1.281$ $E_{pIIa'} = -1.088$
1,4-Dinitrobenzene (**III**)	$E_{pIc} = -1.147$ $E_{pIIc} = -1.279$	$E_{pIa} = -1.073$ $E_{pIIa} = -1.191$
Methyl 3,5-dinitrobenzoate (**IV**)	$E_{pIc} = -1.215$ $E_{pIIc} = -1.620$	$E_{pIa} = -1.138$ $E_{pIIa} = -1.523$

are dependent on the relative positions of the nitro groups in the molecule. Whereas, the coupling between the unpaired electron and the N-nuclei shows the usual triplet pattern that results from coupling of the unpaired electron with two equivalent spin-1 nuclei for all compounds. More specifically, in the case of 1,2-dinitrobenzene (**I**), the observed ESR spectrum (Fig. 3A) consisted of three different *a*-values (Table 2), two of them (two triplet structures) being assigned to the coupling between the unpaired electron with the magnetically equivalent hydrogen atoms (H-nuclei) at positions C-3 and C-6, and to H-nuclei at positions C-4 and C-5. The remaining observed *a*-value was assigned to the coupling between the electron spin density and the magnetically equivalent N-nuclei of both nitro functions, as two-spin-1 triplet structures. Concerning 1,3-dinitrobenzene (**II**), the ESR spectrum (Fig. 3B) is composed by four different *a*-values, in which three of them are related to coupling between the electron spin and the H-nuclei at positions C-2 (doublet), C-4 and C-6 (triplet structure), and C-5 (doublet). Again, coupling with the N-nuclei of the nitro groups was determined by the presence of two-spin-1 equivalent triplet structures. For 1,4-dinitrobenzene (**III**), the experimental ESR pattern (Fig. 3B) showed the presence of two *a*-values: one is assigned to the coupling of the unpaired electron and the H-nuclei at positions C-2, C-3, C-4 and C-5 (quintet structure, all magnetically equivalent), and the other is related to coupling between the N-nuclei of both nitro groups (two triplet spin-1 structures). The *a*-values along with other ESR data are presented in Table 2.

The observed behavior is consistent with the one reported for reduction of dinitro compounds, where the first electron uptake leads to the formation of a radical anion, (Eq. (1)) [5], in which both nitro functions are magnetically equivalent [25]. In order to evaluate the effect that the addition of a second electron in the structure provokes, the ESR experiments were performed applying potential values more negative than the corresponding peak IIc for each molecule (Fig. 2). The resulting ESR spectra are presented in Fig. 4.

Upon reduction at potential values more negative than the corresponding peaks IIc (Fig. 2), for compounds **I** and **III**, the signal proceeding from the first reduction step is not consumed at the applied potential value (Fig. 4A and C); which implies that no consumption of the radical anion was observed. However, in the case of compound **II**, a decrease in the intensity of the ESR signal is observed (Fig. 4B), followed by evolution of this radical species into a secondary radical anion. This behavior was confirmed from the changes in HFCC patterns during power modulation experiments (Fig. 5). After total electrolysis, both species are consumed giving rise to a dianion species.

The presented behavior suggests that, for compounds **I** and **III**, there is another pathway for the formation of the original radical anion structure upon applying potential values more negative than the corresponding peak IIc (Fig. 2A and C). Such behavior has not been considered earlier in the literature dealing with the electrochemical reduction of both compounds. In order to explain the experimental observations, it is considered that, since at this potential condition, the electrogenerated species are the corresponding dianion structures (Eq. (2)), the presence of a comproportionation process [42] would be occurring (Eq. (3)):

$$A^{2-} + A \rightarrow 2A^{\bullet -} \quad (3)$$

This comproportionation process is a thermodynamically necessary condition for reversible EE process affording the dianionic species A^{2-}. Considering the fact that this process involves the electron exchange between A^{2-} and A within the diffusion layer,

Table 2
Hyperfine coupling constants (*a*) in Gauss, linewidths (Γ) in Gauss and isotropic *g*-tensors for the electrogenerated radical anion structures for compounds **I–IV**[a].

	I	**II**	**III**	**IV**
Experimental data				
a_N	2.98	4.32	1.68	4.01
a_2	H-3 = H-6: 0.28	H-2: 1.08	H-2 = H-3 = H-5 = H-6: 1.10	H-2 = H-6: 4.01
a_3	H-4 = H-5: 1.65	H-4 = H-6: 4.45	NA	H-4: 3.31
a_4	NA	H-5: 2.98	NA	NA
Γ	0.12	0.18	0.29	0.34
g	2.0087	2.0084	2.0089	2.0089
Quantum chemical data[b]				
a_N	0.25 (0.56) {0.64}	0.68 (0.90) {1.13}	0.18 (0.34) {0.27}	1.74/1.92 (2.20/2.43) {0.97/1.01} [1.78 (2.45)]
a_2	H-3 = H-6: 0.56 (−0.06) {0.23}	H-2: 0.01 (−0.12) {−0.17}	H-2 = H-3 = H-5 = H-6: −0.94 (−0.92) {−0.94}	H-2/H-6: −7.58/−7.35 (−7.54/−7.36) {−5.48/−5.37} [−7.35 (−7.38)]
a_3	H-4 = H-5: −1.86 (−1.36)	H-4 = H-6: −7.43 (−7.42)	NA	H-4: −0.03 (−0.12) [0.12 (0.02)]
a_4	NA	H-5: 2.13 (2.22) {0.88}	NA	NA
g[c]	2.0053	2.0045	2.0055	2.0045

[a] Assignments for each hyperfine coupling constant with the corresponding hydrogen atom are indicated for each signal (see Fig. 1 for numbering); NA: not applicable.
[b] UB3LYP/EPR-III//UB3LYP/6-311++G(d,p) results, values in parentheses are UB3LYP/EPR-III-PCM results, values in curly brackets are PWP86/6-311++G(2df,p)-C-PCM results, and values in brackets refer to calculations for the perpendicular conformation of the COOMe group.
[c] BLYP/TZ2P-ZORA-SO-COSMO results.

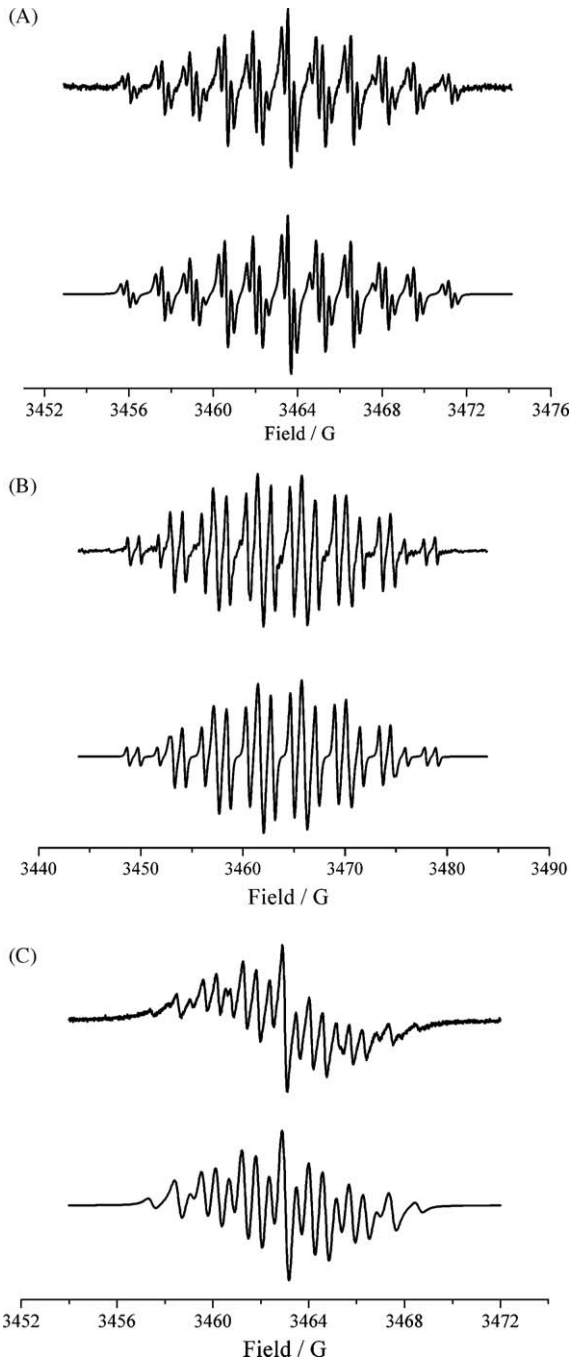

Fig. 3. ESR spectra for the electrogenerated radical species of 1×10^{-3} mol L^{-1} (A) **I**; (B) **II** and (C) **III** in 0.1 mol L^{-1} Et_4NBF_4/CH_3CN. $E_{appl} = -1.35$ V *vs.* Fc^+/Fc (**I**); -1.45 V *vs.* Fc^+/Fc (**II**); -1.20 V *vs.* Fc^+/Fc (**III**). Modulation amplitude: 0.05 G. Upper lines are the corresponding experimental spectra, while lower lines indicate simulated spectra from *a*-values experimentally evaluated.

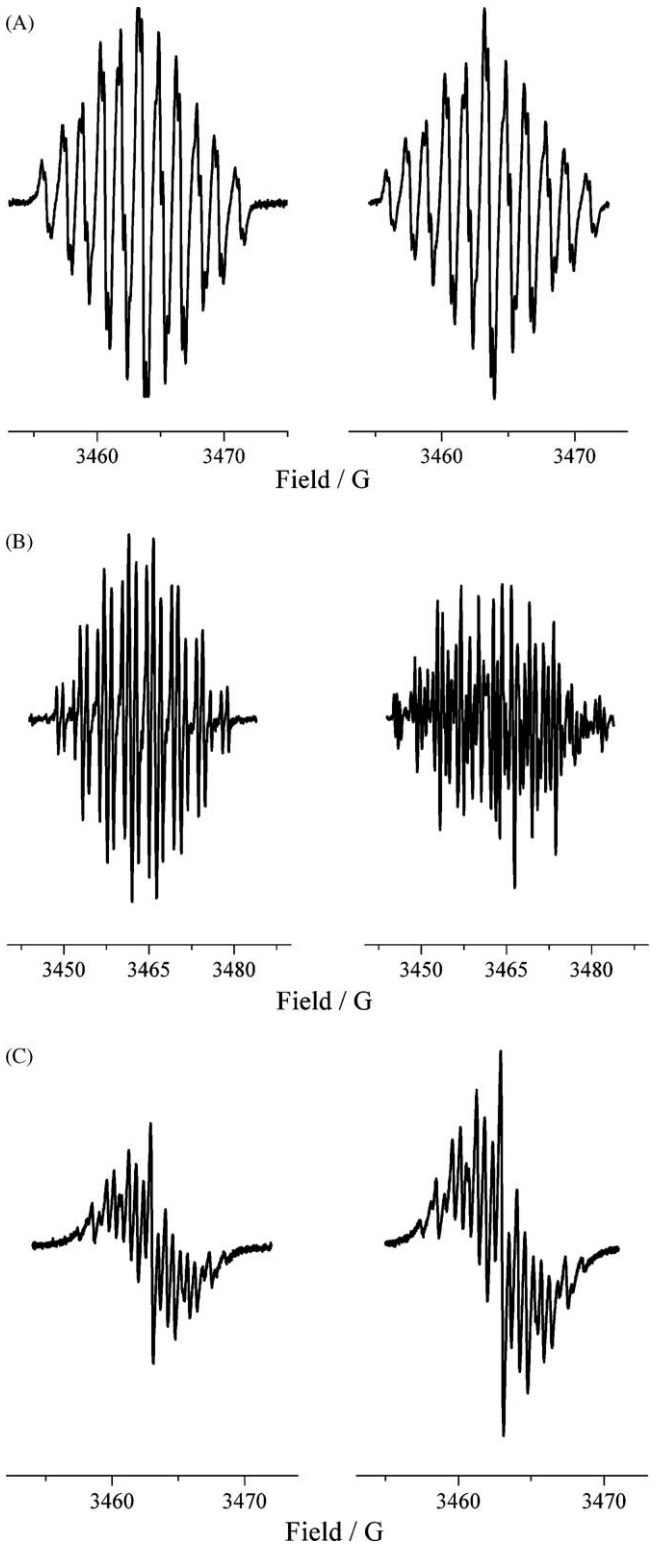

Fig. 4. ESR spectra for the electrogenerated radical species of 1×10^{-3} mol L^{-1} (A) **I**; (B) **II** and (C) **III** in 0.1 mol L^{-1} Et_4NBF_4/CH_3CN. (A) Left ESR spectrum: obtained in $E_{appl} = -1.35$ V *vs.* Fc^+/Fc; right ESR spectrum: obtained in $E_{appl} = -1.60$ V *vs.* Fc^+/Fc. (B) Left ESR spectrum: obtained in $E_{appl} = -1.45$ V *vs.* Fc^+/Fc; right ESR spectrum: obtained in $E_{appl} = -1.85$ V *vs.* Fc^+/Fc. (C) Left ESR spectrum: obtained in $E_{appl} = -1.20$ V *vs.* Fc^+/Fc; Right ESR spectrum: obtained in $E_{appl} = -1.45$ V *vs.* Fc^+/Fc. Modulation amplitude: 0.1 G.

even on the second wave the reaction product is the anion radical $A^{\bullet -}$. Such comproportionation is however modified under long time electrolysis experiments, because concentration of neutral species A is exhausted. Because this process requires the interaction between species A^{2-} and A in the forward direction or two molecules of $A^{\bullet -}$ in the backward direction, it is diffusion limited and is therefore difficult to identify from classic voltammetric experiments [43,44]. However, using the presented spectroelectrochemical approach, it was possible to verify the formation of the radical anion by this comproportionation pathway upon selective detection of the radical species being

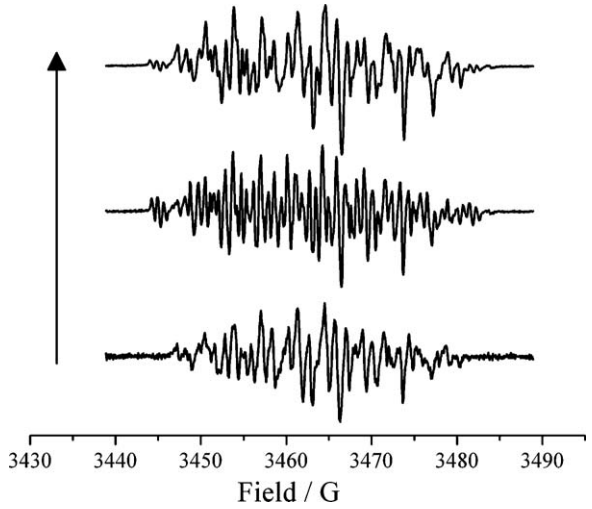

Fig. 5. ESR spectra for the electrogenerated radical species of 1×10^{-3} mol L^{-1} of **II** under increasing irradiating microwave power (0.2, 2 and 20 mW). Arrow indicates the direction of increase of microwave power. $E_{appl} = -1.85$ V *vs.* Fc$^+$/Fc.

generated indirectly from the electrogeneration of the dianionic species.

The case of compound **II** suggests that, during the formation of the corresponding dianion at peak IIc (Fig. 2B), a secondary radical structure (B$^\bullet$) appears. The presence of this secondary radical species has not been considered in earlier discussions of the reactivity of compound **II**. This is probably due to it is consumed during the proceeding electrolysis and the main mechanism observed would be described by Eqs. (1) and (2). Although the corresponding hyperfine patterns could not be deconvoluted from spectra obtained at different irradiated power, thus hindering its structural analysis, this radical species would be formed by interaction between adjacent radical structures, as it has been described in 1,3-disubstituted nitrobenzenes, where there is a possibility of interaction by π-stacking, during the formation of the corresponding radical anion [45].

3.2. Electrochemistry and ESR-spectroelectrochemistry of methyl 3,5-dinitrobenzoate

A similar sequence of experiments was performed with methyl 3,5-dinitrobenzoate (**IV**). The voltammograms obtained for a 1×10^{-3} mol L^{-1} solution of this compound are presented in Fig. 6.

The voltammetric behavior of **IV** is comparable with the one presented by compounds **I**–**III**, characterized by the presence of two one-electron reduction processes, being the first and the second processes electrochemically quasi-reversible ($E_{pIa} - E_{pIc} = 77$ mV; $E_{pIIa} - E_{pIIc} = 97$ mV, Table 1). An extension of the voltammogram towards more negative potential values showed the presence of a third reduction signal of irreversible behaviour, peak IIIc, which is related to the oxidation peak IIIa.

The obtained ESR spectrum during *in situ* spectroelectrochemical experiments applying a potential more negative than peak Ic ($E_{appl} = -1.30$ V *vs.* Fc$^+$/Fc), showed the presence of a stable radical anion species (Fig. 7).

The experimental ESR spectrum is consistent with the presence of three HFCC values: one assigned to coupling between the unpaired electron and the N-atom of the reduced nitro functions at positions 3 and 5. The remaining HFCC values are related to coupling of the electron spin and the H nuclei at positions H-2 and H-6 (triplet) and H-4 (doublet). As occurred for dinitrobenzenes discussed before, the first electron transfer process leads to the formation of a radical anion species where both nitro groups are

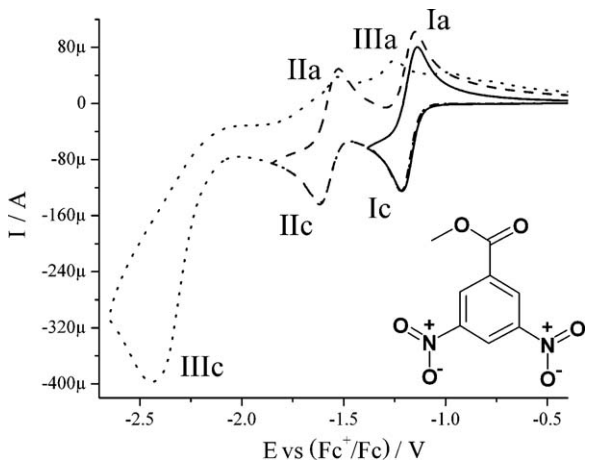

Fig. 6. Cyclic voltammograms of 1×10^{-3} mol L^{-1} of **IV** in 0.1 mol L^{-1} *n*-Bu_4NPF_6/CH_3CN. Voltammograms at different inversion potential conditions are shown. ν: 100 mV s^{-1}. WE: glassy carbon (0.07 cm^2).

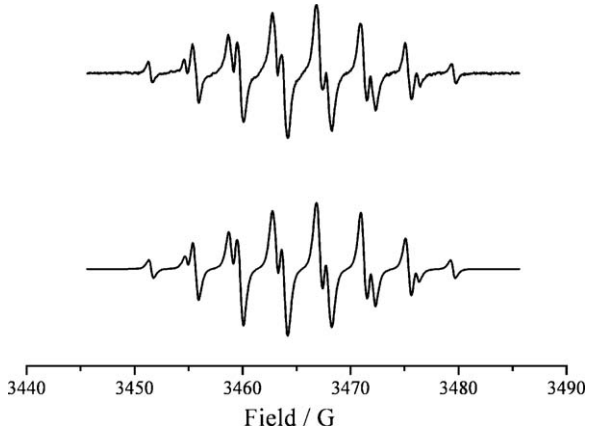

Fig. 7. ESR spectrum for the electrogenerated radical species of 1×10^{-3} mol L^{-1} of **IV** in 0.1 mol L^{-1} Et_4NBF_4/CH_3CN. $E_{appl} = -1.30$ V *vs.* Fc$^+$/Fc. Modulation amplitude: 0.05 G. Upper line is the corresponding experimental spectra, while lower line indicates simulated spectrum from *a*-values experimentally evaluated.

magnetically equivalent [5,25]. As for the cases commented above, the ESR spectroelectrochemical experiments were also performed during application of potential values more negative than for the corresponding reduction signal IIc (Fig. 6). In this case, no diminution of the original ESR signal was observed and the appearance of a secondary radical species was evidenced upon subtracting the spectrum obtained during the previous reduction process (Fig. 6), from the spectrum generated at the applied potential condition. This process is depicted in Fig. 8.

The mixture of radical species obtained during the ESR spectroelectrochemical analysis was evidenced upon performing experiments at different irradiating microwave power (Fig. 9). However, this mixture of radicals did not decay during the experiment – upon passing one equivalent of charge to the solution – differently from the behavior of 1,3-dinitrobenzene (**II**), under similar conditions. The original radical is consumed at potential values more negative than that peak IIc (Fig. 6), and the ESR pattern is similar to the one presented for the subtraction indicated above (Fig. 8C). The pattern presented in Fig. 8C could not be described by a corresponding hyperfine structure, due to the presence of spurious lines originated from the substraction process (see above). However, the regularity of the pattern indicates that these signals are related to a stable radical species, with a different structure to the one obtained in Fig. 8A.

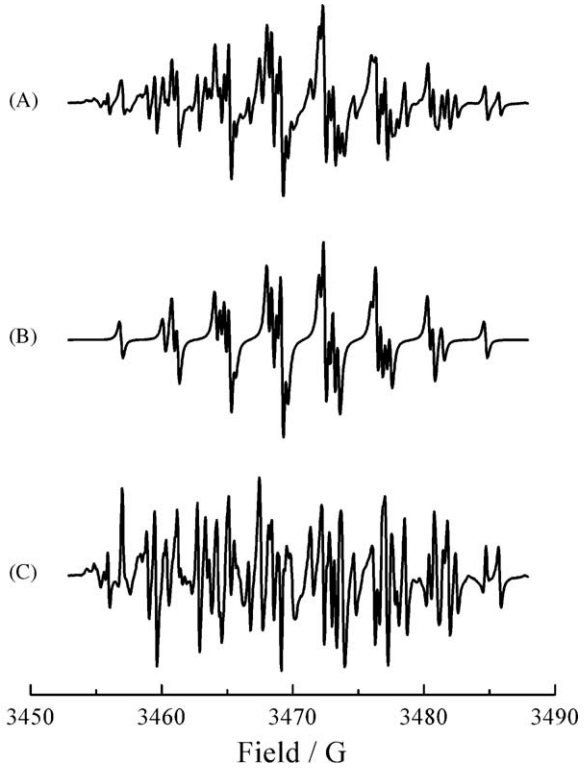

Fig. 8. (A) ESR spectrum for the electrogenerated radical species of 1×10^{-3} mol L^{-1} of **IV** in 0.1 mol L^{-1} Et_4NBF_4/CH_3CN. $E_{appl} = -1.70$ V *vs.* Fc^+/Fc. Modulation amplitude: 0.05 G. (B) Simulated spectrum based upon the result obtained upon reduction at $E_{appl} = -1.30$ V *vs.* Fc^+/Fc. (C) Resultant spectrum from subtracting structure of (B) from (A). Ordinate scale for spectrum C is three times less than for spectra A and B.

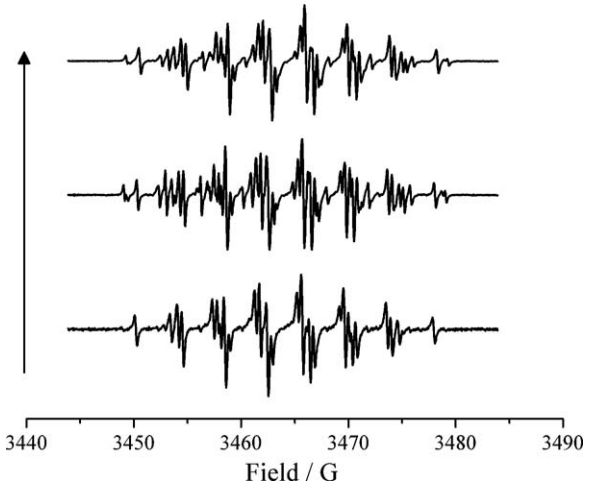

Fig. 9. ESR spectra for the electrogenerated radical species of 1×10^{-3} mol L^{-1} of **IV** under increasing irradiating microwave power (0.2, 2 and 20 mW). Arrow indicates the direction of increase of microwave power. $E_{appl} = -1.70$ V *vs.* Fc^+/Fc.

To explain the behavior above described, the structure of **IV** will be considered as A–A–B, where A represents a nitro group and B represents the carbonyl of the ester function. In this way, the first reduction step carried out at peak Ic, concerns the formation of the radical species $(A^{\bullet -})$–A–B. Owing to the electro-withdrawing power of both nitro groups, the reduction of the carbonyl in the ester function occurs at the level of peak IIc, giving rise to a stable biradical structure $(A^{\bullet -})$–A–$(B^{\bullet -})$, such as it was revealed by the ESR spectra, in which the signal intensity of the moiety $(A^{\bullet -})$ remains constant while it is increased the signal of the alternative radical, assigned to the moiety $(B^{\bullet -})$.

$$A\text{–}A\text{–}B + e^- \rightarrow (A^{\bullet -})\text{–}A\text{–}B \quad \text{Peak Ic} \tag{4}$$

$$(A^{\bullet -})\text{–}A\text{–}B + e^- \rightarrow (A^{\bullet -})\text{–}A\text{–}(B^{\bullet -}) \quad \text{Peak IIc} \tag{5}$$

$$(A^{\bullet -})\text{–}A\text{–}(B^{\bullet -}) + e \rightarrow (A^{2-})\text{–}A\text{–}(B^{\bullet -})\, E_3^0 \tag{6}$$

The irreversible behavior observed at peak IIIc, associated to the formation of the dianion A^{2-}, indicates that the molecule is further reduced; considering the reduction of nitro compounds in non-aqueous media, this electron uptake could be related to the generation of an hydroxylamine derivative (Eq. (7)) [46].

$$(A^{2-})\text{–}A\text{–}(B^{\bullet -}) + 2e^- + 4H^+ \rightarrow (AHOH)\text{–}A\text{–}(B^{\bullet -}) + H_2O \tag{7}$$

This hydroxylamine derivative is the one being oxidized at peak IIIa, forming the corresponding nitroso derivative. It should be noticed that, upon inversion of the potential scan at potential values more negative than peak IIIc, the oxidation process IIa is still visible, while peak Ia disappears (Fig. 6). This behavior is consistent with the presented mechanism of reduction of this compound.

Both radical species behave independently in the same structure, as already described for the reduction of independent redox centers that also generate stable biradical dianionic species [47]. This independent behavior of both radical species indicates that inductive effects which allow the transport of electrons from the reduced sites do not allow a proper coupling of the electron spins being added upon reduction of the respective sites in the molecule (at $-NO_2$ groups at positions C-3 and C-5 and the $COOCH_3$ function at C-1), which would not be the case if resonant effects were present (as in *ortho* or *para* substituted compounds). Also the formation of hydroxylamine is in accordance with the fact that peak IIIc is related to the formation of (A^{2-})–A–$(B^{\bullet -})$ instead of $(A^{\bullet -})$–$(A^{\bullet -})$–$(B^{\bullet -})$. However, a full description of the corresponding hyperfine structure was not possible due to interference from the signals proceeding from the first electrogenerated radical anion. This topic is being currently studied in order to describe the spectral lines of the secondary radical.

3.3. Quantum chemical description of dinitrobenzene derivatives

The experimental results indicate that, even though the first reduction peak for dinitrobenzenes leads to stable radical anions, there are significant differences on the fate of their corresponding forthcoming reductions, for example, the formation of secondary radicals (open-shell electronic structures) or dianions. In particular, for methyl 3,5-dinitrobenzoate (**IV**), ESR signals from radical anion and biradical dianion species are detected, showing that both groups behave as if they were isolated in the molecule. Thus, the structural and electronic properties of compounds **I**, **II**, **III** and **IV** were calculated with quantum chemical methods in order to correlate, to corroborate and to rationalize their spectral and electrochemical behaviors.

3.3.1. Molecular structures and electron affinities of dinitrobenzene derivatives

All the calculated structures of the neutral and radical anions of **I**, **II**, **III** and **IV** with the (U)B3LYP/6-311++G(d,p) method present planar conformations, except **I** that due to the repulsive *ortho* interaction has non-planar conformations of the nitro groups in addition to some deformation of the aromatic ring. The reduction leads to structural changes mainly in the region of the nitro groups in the $\mathbf{I}^{\bullet -}$, $\mathbf{II}^{\bullet -}$ and $\mathbf{III}^{\bullet -}$ species. More specifically, the C–N bonds decrease 5–7 pm, N–O bonds increase 3–4 pm and the C–C bonds near the nitro groups increase 2–3 pm. Also, regarding the structure of $\mathbf{II}^{\bullet -}$ it has been proposed in the literature that its symmetry is broken when computed with UHF and UMP2 methods [48], and it was

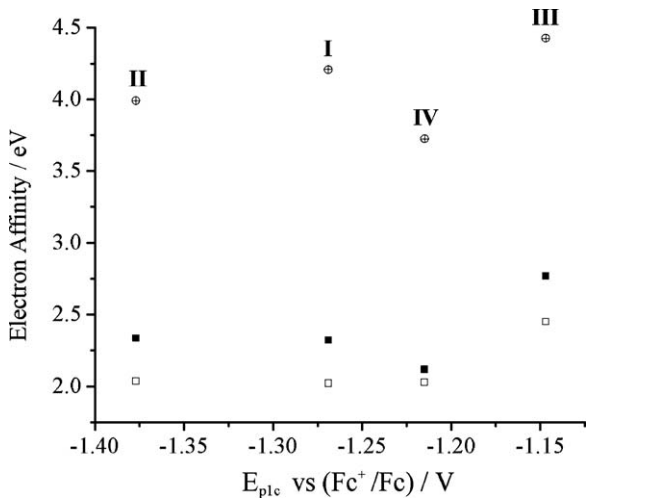

Fig. 10. Correlation between the calculated electron affinities and the first reduction potential for compounds **I**–**IV**. Notation: (□) isolated molecule at the (U)B3LYP/6-311++G(d,p) level; (■) isolated molecule at the (U)B3LYP/EPR-III//(U)B3LYP/6-311++G(d,p) level; (U)B3LYP/EPR-III//(U)B3LYP/6-311++G(d,p) calculations including solvent effects *via* (○) PCM model and (+) C-PCM model.

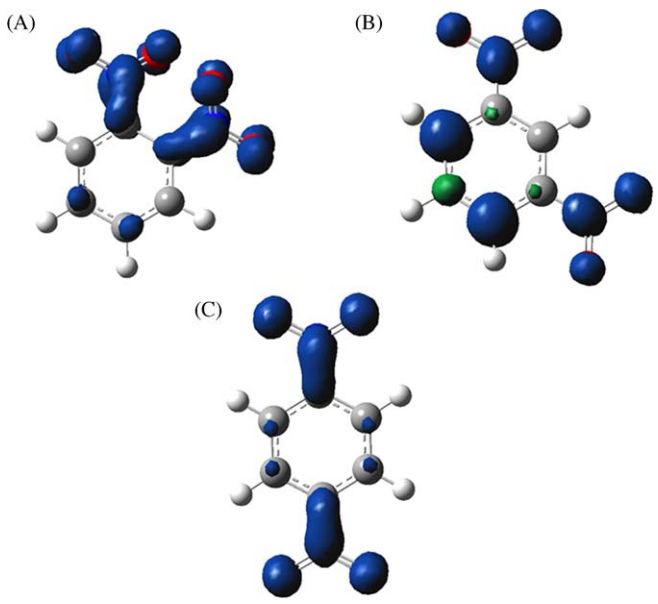

Fig. 11. Spin densities for radical anions from (A) **I**; (B) **II** and (C) **III** using the CPCM model. Isosurfaces are plotted using an isovalue of 0.004 ea_0^{-3}.

rationalized by NBO (Natural Bond Orbital) analysis. However, all DFT functionals tested yielded a symmetric structure for **II**$^{\bullet-}$ and a more detailed analysis of the structures of these radical anions with higher level *ab initio* methods are needed in order to establish the reliability of DFT and UMP2 methods. However, a comparison with the experimental spectral data might also shed some light into these disagreements. Structure **IV**$^{\bullet-}$ also presents a planar conformation, however, due to the asymmetric nature of the COOMe group, the nitro groups become non-equivalent. So, the structure considering the perpendicular conformation of the COOMe group was also calculated. For **IV**$^{\bullet-}$, the calculated structural changes have very similar trends as those in **I**$^{\bullet-}$, **II**$^{\bullet-}$ and **III**$^{\bullet-}$ species, and the only difference is a 2 pm increase in the C–OMe bond length. Whereas, upon further reduction, the **IV**$^{\bullet\bullet 2-}$ triplet radical species presents larger structural changes in the COOMe region, namely, the C–COOMe bond distance decreases 2 pm and the C–OMe bond increases by 3 pm compared to the **IV**$^{\bullet-}$ structure. These results are an indication that the first electron is mainly located in the nitro groups region, whereas the second electron has some delocalization on the C–COOMe region. The double reduced species **IV**$^{2-}$ can also have a singlet spin multiplicity, so its structure was also determined. Indeed, this singlet species has larger structural changes than the triplet one. This is reflected into their relative stabilities, where the triplet species is calculated to be 72.4 kJ mol^{-1} more stable than the singlet optimized structure. These results corroborate the observed ESR signal for the **IV**$^{\bullet\bullet 2-}$ species.

The adiabatic electron affinities (EAs) were calculated as the energy difference between the anionic optimized structure and the neutral optimized structure. These same structures were employed in the calculations of EAs with the EPR-III basis sets as well as with the inclusion of solvent effects via PCM and C-PCM models. Indeed, the solvent effects are quite important for these quantities, however the calculated values are independent of the solvent model used. A good correlation between the first reduced potentials and EAs was obtained for **I**, **II** and **III** when the solvent effects are taken into account. These comparisons are shown in Fig. 10. Note that for compound **IV**, the calculated EA deviates from the correlation obtained for **I**, **II** and **III**. This is probably due to specific interactions between the electrolyte solution and the COOMe group and/or different surface effects (adsorption, orientation, etc.) on the **I**, **II** and **III** series compared to **IV**.

3.3.2. Spin densities and ESR parameters of dinitrobenzene derivatives

Ab initio and density functional theory (DFT) electronic structure methods have been extensively employed in the interpretation, assignment and explanation of reduction potentials and ESR spectra [49–53]. For instance, these methods can yield ESR parameters such as the hyperfine coupling constants as well as the *g*-tensor with high accuracy [49]. However, these calculated ESR parameters are quite dependent upon the theoretical level employed, namely, electronic correlation, DFT functional and basis sets [51]. Usually, pure generalized gradient approximation (GGA) functionals such as BLYP are known to underestimate the calculated ESR parameters, due to underestimation of the spin polarization effects, whereas the unrestricted Hartree–Fock (UHF) method overestimates these properties. These considerations can partially explain (error cancellation) the success of hybrid functionals, that combine GGA and UHF contributions for the exchange functional, such as B3LYP, and allow the determination of ESR parameters more accurately [49]. Also, a correct selection of basis sets is very important since a large contribution for the isotropic HFCC is related to the spin density at the nuclei, thus requiring specialized (EPR-II, EPR-III) or very large Gaussian basis sets (triple and quadruple zeta with polarization functions) or large STO basis sets [51,52]. In addition, solvent effects are quite important for correlating the calculated ESR parameters with the experimental spectra. It has been shown [49] that dielectric continuum models such as PCM and COSMO can take into account the solvent effects on ESR parameters quite satisfactory. Given the size of the radicals studied, the UB3LYP/EPR-III method with the PCM and C-PCM dielectric continuum models were selected for the calculations of spin densities and ESR parameters.

In general, the spin densities (Fig. 11) are mostly located on the nitro groups in **I**$^{\bullet-}$ and **III**$^{\bullet-}$ radicals, whereas for the **II**$^{\bullet-}$ radical a large localization at C-4 and C-6 is also observed (Fig. 11). Addition of the COOMe group (**IV**$^{\bullet-}$ species, Fig. 12A) does not change the spin density pattern observed in the **II**$^{\bullet-}$ radical, since a large localization at C-2 and C-6 is observed in addition to spin localization at the nitro groups. Some spin densities are also observed at C-4 and C-5 in **I**$^{\bullet-}$ and, due to symmetry, at C-2, C-3, C-5 and C-6 in **III**$^{\bullet-}$, where all these spin densities are α-type. This pattern

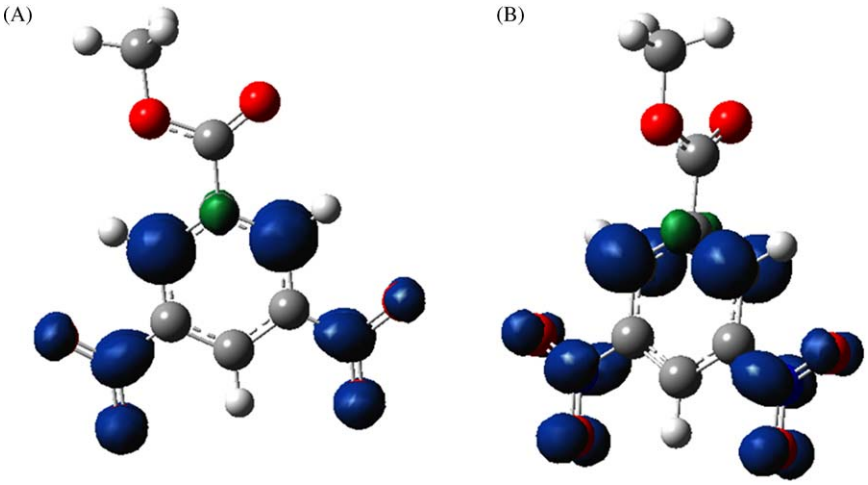

Fig. 12. Spin densities for radical anion from **IV** (A) in planar conformation; (B) in perpendicular conformation, using the CPCM model. Isosurfaces were plotted using an isovalue of 0.004 ea_0^{-3}.

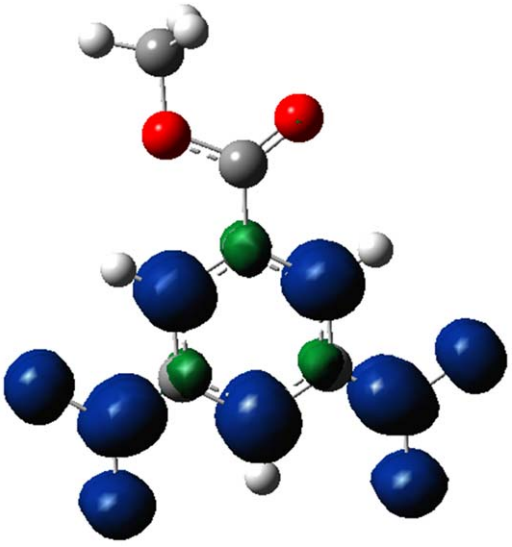

Fig. 13. Spin densities for biradical dianion structure of **IV** using the CPCM model. Isosurface was plotted using an isovalue of 0.004 ea_0^{-3}.

changes for the **II**$^{\bullet-}$ and **IV**$^{\bullet-}$ radicals where some β-type spin density is calculated at C-5 and, equivalently, at C-1, respectively. The perpendicular conformation of the COOMe group (Fig. 12B) does not alter the analysis for the **IV**$^{\bullet-}$ radical, however, the solvent effects do change visually the spin densities in all radical species studied. These changes will be reflected in the calculated values for the HFCC.

Regarding the calculated values for the HFCC, they are included in Table 2 along the experimental ones. As anticipated, the solvent effects can be quite large for calculated *a*-values, including sign changes. Overall, the calculated *a*(H)-values agree quite well with the experimental results and corroborate the assignments. In fact, additional calculations at the PWP86/6-311++G(2df,p) level [54,55] were performed (see Table 2) and improvements were obtained for the *a*(H)-values. The PWP86/6-311G(2df,p) method has the best overall performance for yielding HFCCs of 22 substituted benzene radicals [56]. It should be noted that despite this method underestimates the *a*(H)-values by 5–15%, for the case of 2-nitrophenoxyl radical some values were near 50% in error, and most importantly the relative differences between nuclei adjacent to the nitro group were not consistently reproduced.

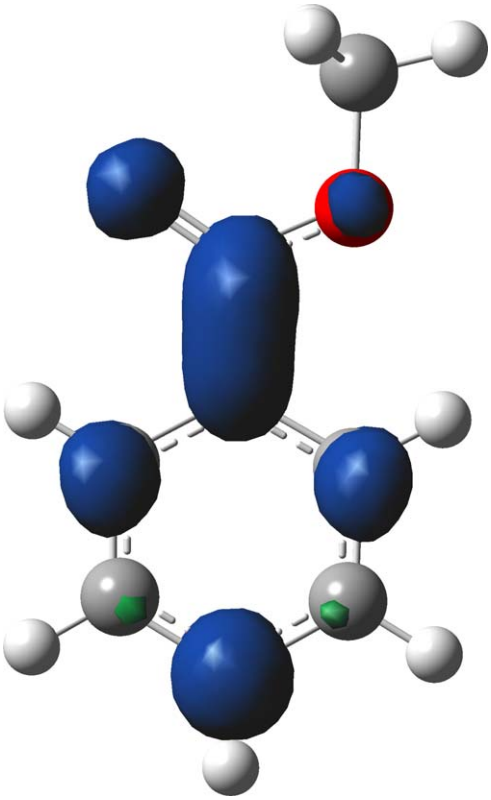

Fig. 14. Spin densities for methyl-benzoate ($C_6H_5COOCH_3$) radical anion using the C-PCM model. Isosurface was plotted using an isovalue of 0.004 ea_0^{-3}.

This suggests that a nitro group can introduce distortions in the molecular electronic densities that are not properly described by popular density functionals. In addition, this systematic study [56] employed only neutral radicals. So, the results presented in Table 2 can be considered fair, but consistent, and further systematic studies of electronic structure methods for describing nitroaryl radical anions are needed. The calculations underestimate quite significantly the *a*(N)-values and yield the corrected ordering only when the solvent effects are included. These quantitative discrepancies were expected from available calculations [57–60] on nitroxide radicals for which the *a*(N)-values are underestimated by 50% or more using widely tested functionals. These

deficiencies are probably due to basis set incompleteness and/or the inability to describe properly the differential spin polarization of different shells by thermodynamically parametrized functionals [58]. The calculated isotropic *g*-tensor is also underestimated, but since they represent a global property originating from very fine relativistic corrections, quantitative agreement between the calculated and experimental values would not be expected. However, the calculated values correlate very well with the experimental data, including the relative differences between the dinitrobenzene studied.

In addition, despite the ESR parameters for the $\mathbf{IV}^{\bullet\bullet 2-}$ triplet species not being determined, they were calculated with the same method and yielded the following predictions for the *a*-values (in Gauss): *a*(N-3) = 2.79 (3.42); *a*(N-5) = 2.85 (3.43); *a*(H-2) = −3.42 (−3.42); *a*(H-6) = −3.47 (−3.41); *a*(H-4) = −4.96 (−4.33), where the values in parentheses include the solvent effects via PCM model. The corresponding spin density is presented in Fig. 13, which can be compared to the spin densities presented in Figs. 11 and 12, as well as the spin density of methylbenzoate radical anion presented in Fig. 14. These comparisons allow a qualitative view of the effects of the substituents (nitro *vs*. ester) on the spin densities of radical anion and biradical dianion.

4. Conclusions

In this work, the effect of the relative positions of the nitro groups (*ortho vs. para vs. meta*) during reduction of dinitrobenzenes was analysed. Cyclic voltammetry experiments in acetonitrile solution revealed that *ortho*-, *meta*- and *para*-dinitrobenzenes (**I**, **II**, **III**) show two reversible reduction processes. An Electrochemical-Electron Spin Resonance (E-ESR) study showed that the corresponding radical anions of the *ortho* and *para* derivatives, electrogenerated during the first electron transfer uptake can be reduced to a dianionic form, whose interaction with the neutral species give rise to a comproportionation reaction ($A^{2-} + A \rightarrow 2A^{\bullet -}$), which allows to increase the population of the initial radical anions. This reaction is driven by stability of the corresponding radical anions, which is favoured by the adequate interactions between both nitro groups. Such situation is only partially valid for the case of the *meta* derivative, whose radical anion, electrogenerated at the first reduction peak, is consumed at the second reduction step, forming a secondary radical species. During the study of the methyl 3,5-dinitrobenzoate (**IV**), two successive and quasi-reversible electron processes were also observed; however, in this case, a very rare biradical structure was found, in which the carbomethoxy and nitro group are independently reduced. The use of E-ESR shed some light on controversial aspects of nitroaromatic reduction, especially concerning the second and further waves. Quantum chemical calculations have successfully corroborated, rationalized and explained most electrochemical and spectral results, however, systematic studies addressing the performance of electronic structure methods for treating nitroaryl radical anions are needed.

Acknowledgments

L.S. Hernández-Muñoz thanks CONACyT-Mexico for funding of her Ph.D. studies. The Brazilian agencies CNPq, CAPES, CASADINHO/CNPq, FAPEAL, FACEPE, FINEP, INCT-Bioanalítica, INAMI and RENAMI are acknowledged for grants and fellowships. The authors deeply thank Prof. Christian Amatore (ENS – Paris) for fruitful discussions, concerning comproportionation. Also Mr. Marcus V.P. dos Santos is acknowledged for performing some computer calculations.

References

[1] H. Lund, in: H. Lund, O. Hammerich (Eds.), Organic Electrochemistry, 4th ed., Marcel Dekker, New York, 2001, Ch. 9.
[2] J.H. Tocher, D.I. Edwards, Biochem. Pharmacol. 50 (1995) 1367.
[3] F.C. De Abreu, J. Tonholo, O.L. Bottecchia, C.L. Zani, M.O.F. Goulart, J. Electroanal. Chem. 462 (1999) 195.
[4] F.C. De Abreu, F.S. De Paula, A.F. Dos Santos, A.E.G. Sant'ana, M.V. De Almeida, M.O.F. Goulart, Bioorg. Med. Chem. 9 (2001) 659.
[5] N. Arshad, N.K. Janjua, S. Ahmed, A.Y. Khan, L.H. Skibsted, Electrochim. Acta 54 (2009) 6184.
[6] A.S. Mendkovich, M.A. Syroeshkin, L.V. Mikhalchenko, A.I. Rusakov, V.P. Gultyai, Russ. Chem. Bull. 57 (2008) 1492.
[7] M.M. Islam, T. Okajima, T. Ohsaka, J. Electroanal. Chem. 618 (2008) 1.
[8] N.A. Macías-Ruvalcaba, J.P. Telo, D.H. Evans, J. Electroanal. Chem. 600 (2007) 294.
[9] R.L. Ward, J. Chem. Phys. 32 (1960) 410.
[10] F.C. de Abreu, P.A.M. Ferraz, M.O.F. Goulart, J. Braz. Chem. Soc. 13 (2002) 19.
[11] J.A. Squella, S. Bollo, L.J. Núñez-Vergara, Curr. Org. Chem. 9 (2005) 565.
[12] M.O.F. Goulart, A.A. De Souza, F.C. De Abreu, F.S. De Paula, E.M. Sales, W.P. Almeida, O. Buriez, C. Amatore, J. Electrochem. Soc. 154 (2007) P121.
[13] A.H. Maki, D.H. Geske, J. Am. Chem. Soc. 83 (1961) 1852.
[14] D.H. Geske, J.L. Ragle, M.A. Bambenek, A.L. Balch, J. Am. Chem. Soc. 86 (1964) 987.
[15] I. Bernal, G.K. Fraenk, J. Am. Chem. Soc. 86 (1964) 1671.
[16] R.G. Compton, R.A.W. Dryfe, J. Electroanal. Chem. 375 (1994) 247.
[17] T. Kitagawa, T.P. Layloff, R.N. Adams, Anal. Chem. 35 (1963) 1086.
[18] L. Horner, H. Newmann, Chem. Ber. 98 (1965) 3462.
[19] R. Labrecque, J. Mailhot, J.M. Daoust, J.M. Chapuzet, J. Lessard, Electrochim. Acta 42 (1997) 2089.
[20] D.L. Kirkpatrick, K.E. Johnson, A.C. Sartorelli, J. Med. Chem. 29 (1986) 2048.
[21] S.M.A. Jorge, N.R. Stradiotto, J. Electroanal. Chem. 431 (1997) 237.
[22] F. Ammar, J.M. Savéant, J. Electroanal. Chem. 47 (1973) 115.
[23] M.W. Lehmann, P. Singh, D.H. Evans, J. Electroanal. Chem. 549 (2003) 137.
[24] N.A. Macías-Ruvalcaba, D.H. Evans, J. Phys. Chem. B 109 (2005) 14642.
[25] S.F. Nelsen, A.E. Konradsson, M.N. Weaver, J.P. Telo, J. Am. Chem. Soc. 125 (2003) 12493.
[26] D.K. Roe, in: P.T. Kissinger, W.R. Heineman (Eds.), Laboratory Techniques in Electroanalytical Chemistry, Marcel Dekker, Inc., New York, USA, 1996.
[27] P. He, L.R. Faulkner, Anal. Chem. 58 (1986) 517.
[28] G. Gritzner, J. Küta, Pure. Appl. Chem. 4 (1984) 462.
[29] P.J. Stephens, F.J. Devlin, C.F. Chabalowski, M.J. Frisch, J. Phys. Chem. 98 (1994) 11623.
[30] A.D. McLean, G.S. Chandler, J. Chem. Phys. 72 (1980) 5639;
R. Krishnan, J.S. Binkley, R. Seeger, J.A. Pople, J. Chem. Phys. 72 (1980) 650.
[31] M.J. Frisch, G.W. Trucks, H.B. Schlegel, G.E. Scuseria, M.A. Robb, J.R. Cheeseman, J.A. Montgomery Jr., T. Vreven, K.N. Kudin, J.C. Burant, J.M. Millam, S.S. Iyengar, J. Tomasi, V. Barone, B. Mennucci, M. Cossi, G. Scalmani, N. Rega, G.A. Petersson, H. Nakatsuji, M. Hada, M. Ehara, K. Toyota, R. Fukuda, J. Hasegawa, M. Ishida, T. Nakajima, Y. Honda, O. Kitao, H. Nakai, M. Klene, X. Li, J.E. Knox, H.P. Hratchian, J.B. Cross, C. Adamo, J. Jaramillo, R. Gomperts, R.E. Stratmann, O. Yazyev, A.J. Austin, R. Cammi, C. Pomelli, J.W. Ochterski, P.Y. Ayala, K. Morokuma, G.A. Voth, P. Salvador, J.J. Dannenberg, V.G. Zakrzewski, S. Dapprich, A.D. Daniels, M.C. Strain, O. Farkas, D.K. Malick, A.D. Rabuck, K. Raghavachari, J.B. Foresman, J.V. Ortiz, Q. Cui, A.G. Baboul, S. Clifford, J. Cioslowski, B.B. Stefanov, G. Liu, A. Liashenko, P. Piskorz, I. Komaromi, R.L. Martin, D.J. Fox, T. Keith, M.A. Al-Laham, C.Y. Peng, A. Nanayakkara, M. Challacombe, P.M.W. Gill, B. Johnson, W. Chen, M.W. Wong, C. Gonzalez, J.A. Pople, Gaussian 03, Revision B.04, Gaussian, Inc., Pittsburgh, PA, 2003.
[32] V. Barone, in: D.P. Chong (Ed.), Recent Advances in Density Functional Methods, Part I, World Scientific Publ. Co., Singapore, 1996.
[33] M.T. Cancès, B. Mennucci, J. Tomasi, J. Chem. Phys. 107 (1997) 3032;
M. Cossi, V. Barone, B. Mennucci, J. Tomasi, Chem. Phys. Lett. 286 (1998) 253.
[34] V. Barone, M. Cossi, J. Phys. Chem. A 102 (1998) 1995.
[35] V. Barone, M. Cossi, J. Tomasi, J. Chem. Phys. 107 (1997) 3210.
[36] E. van Lenthe, P.E.S. Wormer, A. van der Avoird, J. Chem. Phys. 107 (1997) 2488.
[37] A.D. Becke, J. Chem. Phys. 98 (1993) 5648;
C. Lee, W. Yang, R.G. Parr, Phys. Rev. B 37 (1988) 785.
[38] ADF Program System, Release 2009.01, Scientific Computing & Modelling NV Vrije Universiteit, Theoretical Chemistry, De Boelelaan 1083; 1081 HV Amsterdam, The Netherlands.
[39] E. van Lenthe, A.E. Ehlers, E.J. Baerends, J. Chem. Phys. 110 (1999) 8943.
[40] E. van Lenthe, J.G. Snijders, E.J. Baerends, J. Chem. Phys. 105 (1996) 6505;
E. van Lenthe, R. van Leeuwen, E.J. Baerends, J.G. Snijders, Int. J. Quant. Chem. 57 (1996) 281.
[41] C. Chan-Leonor, S.L. Martin, D.K. Smith, J. Org. Chem. 70 (2005) 10817.
[42] M.W. Lehmann, D.H. Evans, J. Electroanal. Chem. 500 (2001) 12.
[43] P. Hapiot, L. Kispert, V. Konovalov, J.M. Saveant, J. Am. Chem. Soc. 123 (2001) 6669.
[44] A.J. Bard, L. Faulkner, Electrochemical Methods, Fundamentals and Applications, John Wiley & Sons, USA, 2001, Ch. 12.
[45] I. Gallardo, G. Guirado, J. Marquet, N. Vila, Angew. Chem. Int. Ed. 46 (2007) 1321.
[46] A.J. Fry, in: S. Patai (Ed.), The Chemistry of Amino, Nitroso, Nitro & Related Groups, Supplement F2, Wiley, New York, 1997, p. 837.

[47] D.M. Hernández, M.A.B.F. de Moura, D.P. Valencia, F.J. González, I. González, F.C. de Abreu, E.N. da Silva Junior, V.F. Ferreira, A. Ventura Pinto, M.O.F. Goulart, C. Frontana, Org. Biomol. Chem. 6 (2008) 3414.
[48] S.F. Nelsen, M.N. Weaver, A.E. Konradsson, J.P. Telo, T. Clark, J. Am. Chem. Soc. 126 (2004) 15431.
[49] M. Kaupp, M. Bühl, V.G. Malkin (Eds.), Calculation of NMR and EPR Parameters, WILEY-VCH Verlag GmbH & Co. KGaA, 2004.
[50] F. Neese, J. Chem. Phys. 115 (2001) 11080.
[51] A.R. Jaszewski, Z. Siatecki, J. Jezierska, Chem. Phys. Lett. 331 (2000) 403.
[52] E. Ionescu, S.A. Reid, J. Mol. Struct. Theochem. 725 (2005) 45.
[53] Z. Rinkevicius, L. Telyatnyk, O. Vahtras, H. Ågren, J. Chem. Phys. 121 (2004) 7614.
[54] J.P. Perdew, Y. Wang, Phys. Rev. B 33 (1986) 8800.
[55] J.P. Perdew, Phys. Rev. B 33 (1986) 8822;
J.P. Perdew, Phys. Rev. B 34 (1986) 7406.
[56] L.A. Eriksson, Mol. Phys. 91 (1997) 827.
[57] S.M. Mattar, Chem. Phys. Lett. 300 (1999) 545.
[58] R. Improta, V. Barone, Chem. Rev. 104 (2004) 1231.
[59] R. Owenius, M. Engstrom, M. Lindgren, M. Huber, J. Phys. Chem. A 105 (2001) 10967.
[60] S. Choua, J.-P. Djukic, J. Dallery, A. Bieber, R. Welter, J. Gisselbrecht, P. Turek, L. Ricard, Inorg. Chem. 48 (2009) 149.